Photocurrents of charge and spin in monolayer Fe₃GeTe₂

M. Merte ,[1,2,3,*] F. Freimuth ,[3,1,†] T. Adamantopoulos ,[1] D. Go,[3,1] T. G. Saunderson ,[3,1] M. Kläui,[3]
L. Plucinski,[1] O. Gomonay ,[3] S. Blügel ,[1] and Y. Mokrousov[1,3,‡]

[1]*Peter Grünberg Institut and Institute for Advanced Simulation, Forschungszentrum Jülich and JARA, 52425 Jülich, Germany*
[2]*Department of Physics, RWTH Aachen University, 52056 Aachen, Germany*
[3]*Institute of Physics, Johannes Gutenberg University Mainz, 55099 Mainz, Germany*

In the realm of two-dimensional materials, magnetic and transport properties of a unique representative Fe₃GeTe₂ attract ever increasing attention. Here, we use a developed first-principles method for calculating laser-induced response to study the emergence of photoinduced currents of charge and spin in single-layer Fe₃GeTe₂, which are of second order in the electric field. We provide a symmetry analysis of the emergent photocurrents in the system, finding it to be in excellent agreement with *ab initio* calculations. We analyze the magnitude and behavior of the charge photocurrents with respect to disorder strength, frequency, and band filling. Remarkably, not only do we find a large charge current response, but also predict that Fe₃GeTe₂ can serve as a source of significant laser-induced spin currents, which makes this material as a promising platform for various applications in optospintronics.

Introduction. The tremendous progress in realization of robust two-dimensional (2D) magnetism in van der Waals materials [1–4] moves various properties of 2D magnetic materials into the focus of intense attention. Among the latter, layered Fe₃GeTe₂ (FGT) is one of the most prolific candidates for potential 2D magnetic applications, as it is one of the few compounds among 2D materials that exhibits strong out-of-plane magnetocrystalline anisotropy, has one of the largest Curie temperatures among 2D materials [5], and provides a playground for realization of complex spin textures [6–8]. Current-induced switching of magnetization in FGT has been achieved [9], and it was argued that intrinsic bulklike spin-orbit torques, arising without a need for an interface, can be very large in this material [10,11]. Moreover, it was predicted that FGT displays very prominent Kerr and Faraday effects, with magneto-optical properties being qualitatively similar when going from bulk to the single-layer limit owing to the weak coupling among the layers [12,13]. These findings motivate an extensive further exploration of intrinsic properties of FGT, especially in the area of its magnetic response to electromagnetic fields.

On this front, the properties of laser-ignited charge currents are currently studied very intensively in interfacial systems and 2D materials since they mediate THz radiation [14–17] and carry important information about intrinsic characteristics of the system [17–20]. While it is known that even in nonmagnetic noncentrosymmetric materials such as semiconductors [21,22], quantum wells [23], graphene [24], and organic-inorganic halides [25] light can give rise to spin currents, following the initial suggestion of enhanced surface spin photocurrents in magnetic systems [26], the physics of laser-driven spin currents in 2D magnetic materials has started to attract attention as well [27–29]. In this work we study the properties of laser-induced in-plane charge and spin currents in a single-layer FGT from first principles. For this, we employ an *ab initio* implementation of the expressions for photocurrents of spin and charge that we derived recently [26], which work equally well for insulating and metallic systems of any given complexity, and allow for considering the effect of disorder. We compute the charge and spin current response of FGT for different degree of disorder, and analyze it as a function of frequency and band filling. Our results provide an important reference point for exploring future optospintronics applications of this exciting material.

Method. In order to compute the photocurrents in the system arising as a response to a continuous laser pulse of frequency ω, we employ an expression for the second-order photocurrent density which was previously derived by us using Keldysh formalism [26]:

$$J_i = \frac{a_0^2 e \epsilon_0}{2\hbar} \left(\frac{\varepsilon_{\mathrm{H}}}{\hbar\omega}\right)^2 \mathrm{Im} \sum_{jk} E_j E_k^* \varphi_{ijk}, \qquad (1)$$

where a_0 is the Bohr's radius, e is the elementary charge, $\hbar$ is the reduced Planck constant, $\varepsilon_H = e^2/(4\pi\epsilon_0 a_0)$ is the Hartree energy, and E_i is the ith component of the complex field amplitude of the pulse. The quantity φ_{ijk} is defined as the following energy integral [26]:

$$\varphi_{ijk} = \frac{2}{a_0 \mathcal{E}_{\mathrm{H}}} \int \frac{d^2 k}{(2\pi)^2} \int d\mathcal{E} \, \mathrm{Tr}$$
$$\times \left[f(\mathcal{E}) v_i G_{\boldsymbol{k}}^{\mathrm{R}}(\mathcal{E}) v_j G_{\boldsymbol{k}}^{\mathrm{R}}(\mathcal{E} - \hbar\omega) v_k G_{\boldsymbol{k}}^{\mathrm{R}}(\mathcal{E}) \right.$$

*m.merte@fz-juelich.de
†f.freimuth@fz-juelich.de
‡y.mokrousov@fz-juelich.de

$$- f(\mathcal{E})v_i G_{\boldsymbol{k}}^{R}(\mathcal{E})v_j G_{\boldsymbol{k}}^{R}(\mathcal{E} - \hbar\omega)v_k G_{\boldsymbol{k}}^{A}(\mathcal{E})$$
$$+ f(\mathcal{E})v_i G_{\boldsymbol{k}}^{R}(\mathcal{E})v_k G_{\boldsymbol{k}}^{R}(\mathcal{E} + \hbar\omega)v_j G_{\boldsymbol{k}}^{R}(\mathcal{E})$$
$$- f(\mathcal{E})v_i G_{\boldsymbol{k}}^{R}(\mathcal{E})v_k G_{\boldsymbol{k}}^{R}(\mathcal{E} + \hbar\omega)v_j G_{\boldsymbol{k}}^{A}(\mathcal{E})$$
$$+ f(\mathcal{E} - \hbar\omega)v_i G_{\boldsymbol{k}}^{R}(\mathcal{E})v_j G_{\boldsymbol{k}}^{R}(\mathcal{E} - \hbar\omega)v_k G_{\boldsymbol{k}}^{A}(\mathcal{E})$$
$$+ f(\mathcal{E} + \hbar\omega)v_i G_{\boldsymbol{k}}^{R}(\mathcal{E})v_k G_{\boldsymbol{k}}^{R}(\mathcal{E} + \hbar\omega)v_j G_{\boldsymbol{k}}^{A}(\mathcal{E})], \quad (2)$$

where v_i is the ith component of the velocity operator, $f(\mathcal{E})$ is the Fermi-Dirac distribution function, and $G_{\boldsymbol{k}}^{R/A}$ are equilibrium retarded and advanced Green's functions, respectively. In order to compute the spin photocurrent Q_{si} propagating in direction i and polarized along axis s, we replace the first of the velocity operators v_i appearing in the expression above, with the operator of the spin velocity $\{v_i, \sigma_s\}$, and change the prefactor $a_0^2 e\epsilon_0/2\hbar$ in Eq. (1) to $-a_0^2\epsilon_0/8$.

In this work, we model the effect of disorder by adapting a model of constant lifetime broadening of the states Γ which results in the following expressions: $G_{\boldsymbol{k}}^{R}(\mathcal{E}) = \hbar \sum_n \frac{|kn\rangle\langle kn|}{\mathcal{E} - \mathcal{E}_{kn} + i\Gamma}$ and $G_{\boldsymbol{k}}^{A}(\mathcal{E}) = [G_{\boldsymbol{k}}^{R}(\mathcal{E})]^{\dagger}$ [26], where the energy of the state $|kn\rangle$ in band n with a Bloch vector $\boldsymbol{k}$ is $\mathcal{E}_{kn}$. To compute the photocurrent the integrals in Eq. (2) have to be evaluated. At zero temperature the Fermi distribution becomes a step function which allows one to perform the energy integration analytically [30]. The numerical evaluation is preformed within the basis of maximally localized Wannier functions, and the Brillouin zone integration is performed numerically by employing the efficient technique of Wannier interpolation [31–33]. A more detailed description of the methodology will be published elsewhere. Throughout this work we assume an intensity of the light of 10 GW/cm^2, which corresponds to typical values of the fluence of the order of 0.5 mJ/cm^2 for a 50-fs laser pulse [20].

Computational details. The considered structure of single-layer FGT is shown in Figs. 1(a) and 1(b). Our calculations of single-layer Fe$_3$GeTe$_2$ with point group D_{3h} predict that in agreement with experiments the FGT layer exhibits a ferromagnetic ground state with the easy axis pointing out of the plane when grown at the lattice constant of bulk Fe$_3$GeTe$_2$ [1]. The electronic structure of the system was calculated including the effect of spin-orbit coupling (SOC) with the film version of the FLEUR code [34]. The in-plane lattice constant was set to $a = 7.542$ a.u. For self-consistent calculations we used a plane-wave cutoff of 5.0 a.u.$^{-1}$ and the total of 576 k points in the two-dimensional Brillouin zone. The muffin-tin radii for Fe, Ge, and Te were set to 2.08, 2.19, and 2.40 a.u., respectively. The nonrelativistic Perdew-Burke-Ernzerhoff (PBE) [35] exchange-correlation functional was used. The computed band structure of the system, shown in Fig. 1, reflects the complex orbital interplay around the Fermi energy $\mathcal{E}_F$ typical of FGT. The impact of low symmetry of FGT on the electronic structure can be clearly observed along the K'-Γ-K path in Fig. 1, and it ultimately gives rise to nonvanishing complex nonlinear response. After converging the electronic structure we extracted 48 maximally localized Wannier functions by using Fe d and Ge, Te p orbitals as initial projections since these orbitals dominate the band structure in a wide energy window around E_F. Based on the tight-binding Wannier Hamiltonian constructed from
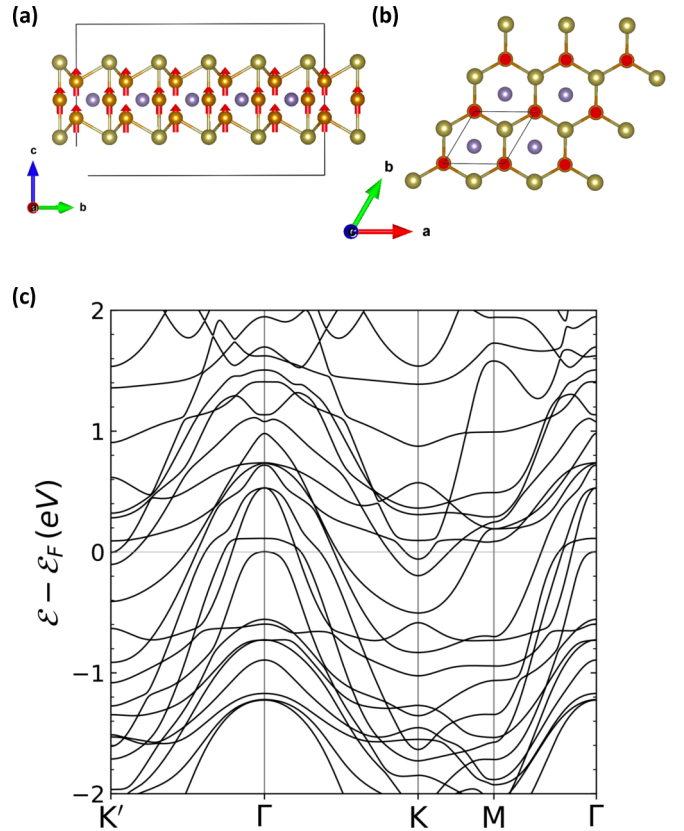

FIG. 1. Geometry and electronic structure of single-layer Fe$_3$GeTe$_2$ (FGT). (a) Side view of FGT layer with red arrows indicating magnetic moments on Fe atoms directed out of plane. (b) Top view of a 2×2 unit cell of single-layer FGT. In (a) and (b) blue spheres, green spheres, and red spheres stand for Ge, Te, and Fe atoms, respectively. (c) Band structure of ferromagnetic FGT layer in a $[-2, +2]$ eV energy window around the Fermi energy.

the Wannier functions we computed the photocurrents on a 2000×2000 interpolation k mesh, which provides well-converged results for the lifetime broadening larger than $\Gamma = 25$ meV.

Symmetry analysis. In order to investigate which constraints are imposed on the photocurrents by the crystal symmetry we expand the photocurrent up to the first order in the magnetization as follows:

$$J_i = 2\sigma_{ijk}E_j E_k^* = \chi_{ijk}E_j E_k^* + \chi_{ijkl}E_j E_k^* M_l, \quad (3)$$

where σ_{ijk} is the photoconductivity tensor, χ_{ijk} is a polar tensor of rank 3, and χ_{ijkl} is an axial tensor of rank 4. We introduce the notation for the basis tensors $\delta_{ijkl}^{(nopq)} = \delta_{in}\delta_{jo}\delta_{kp}\delta_{lq} := \langle nopq \rangle$, which allows us to list the tensors that are permitted by symmetry in a compact form. Only one polar tensor of rank 3 is allowed by symmetry, namely, $\chi_{ijk}^{(p,1)} = \delta_{ijk}^{(xxx)} - \delta_{ijk}^{(yyx)} - \delta_{ijk}^{(xyy)} - \delta_{ijk}^{(yxy)}$, while four axial tensors of rank 4 are consistent with the symmetry: $\chi_{ijkl}^{(a,1)} = -\delta_{ijkl}^{(zyxx)} - \delta_{ijkl}^{(zyxy)} - \delta_{ijkl}^{(zxxy)} + \delta_{ijkl}^{(zyyy)}$, $\chi_{ijkl}^{(a,2)} = -\delta_{ijkl}^{(yxxz)} - \delta_{ijkl}^{(xyxz)} - \delta_{ijkl}^{(xxyz)} + \delta_{ijkl}^{(yyyz)}$, $\chi_{ijkl}^{(a,3)} = -\delta_{ijkl}^{(yxzx)} - \delta_{ijkl}^{(xyzx)} - \delta_{ijkl}^{(xxzy)} + \delta_{ijkl}^{(yyzy)}$, and $\chi_{ijkl}^{(a,4)} = \delta_{ijkl}^{(yzxx)} + \delta_{ijkl}^{(xzyx)} + \delta_{ijkl}^{(xzxy)} - \delta_{ijkl}^{(yzyy)}$. We do not need to consider $\chi^{(a,1)}$ due to
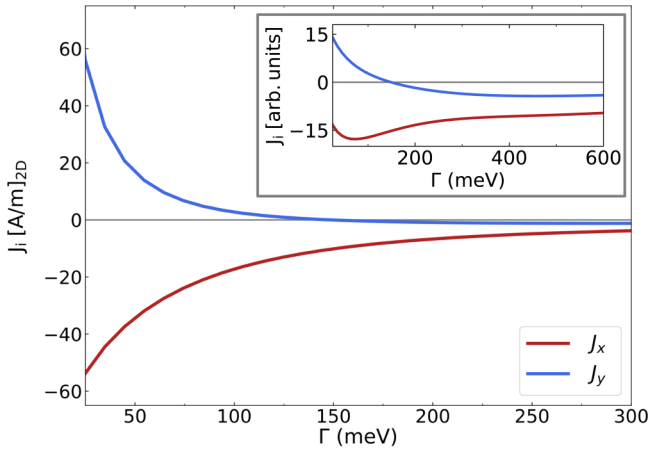
FIG. 2. Dependence of photocurrents on the band broadening Γ. Shown are the photocurrent components J_x (red solid line) and J_y (blue dashed line) in response to the light pulse of frequency $\hbar\omega = 1.55$ eV and intensity of 10 GW/cm^2 polarized along the x axis. The inset depicts the corresponding photocurrent components multiplied with a factor Γ.

the 2D character of FGT, where out-of-plane photocurrents are not of interest. Additionally, we may ignore $\chi^{(a,3)}$ and $\chi^{(a,4)}$ because we choose the magnetization direction along the z axis. Considering the remaining tensors, expressions for $\chi^{(p,1)}$ and $\chi^{(a,2)}$ predict vanishing photocurrents for the circularly polarized pulses, while the sign of J_i switches upon the change in the direction of light from x to y for linearly polarized light. For the spin current we perform a similar symmetry analysis by expanding it as

$$Q_{si} = \chi_{sijk}E_jE_k^* + \chi_{sijkl}E_jE_k^*M_l, \qquad (4)$$

where χ_{sijk} is an axial tensor of rank 4 while χ_{sijkl} is a polar tensor of rank 5. The expressions for axial tensors of rank 4 are listed above, and due to the 2D character of FGT, we need to consider only $\chi^{(a,1)}$ in the expansion of Q_{si} (note that in the expansion of J_i we excluded $\chi^{(a,1)}$). There are 15 polar tensors of rank 5 for the point group of FGT. As discussed above, we need to consider only tensors that predict an effect for magnetization along the z axis. Additionally, we consider only tensors where the indices i, j, k are all different from z because of the 2D character of FGT. It turns out that out of the 15 polar tensors only a single one satisfies these requirements. It is given by $\chi_{sijkl}^{(p,1)} = \delta_{sijkl}^{(zxxxz)} - \delta_{sijkl}^{(zyyxz)} - \delta_{sijkl}^{(zyxyz)} - \delta_{sijkl}^{(zxyyz)}$. As a result, by symmetry only z-polarized spin currents are allowed, with in-plane properties of spin currents identical to those of charge currents.

Results. Overall, within the accuracy of the calculations, the symmetry properties of computed photocurrents are fully consistent with the symmetry analysis presented above, and thus in the following we focus only on J_x and J_y components of the charge current, and Q_{zx} and Q_{zy} components of the spin current, arising in response to a laser pulse polarized along the x direction. First, we calculate and present in Fig. 2 the dependence of the charge photocurrents on the quasiparticle lifetime as quantified by parameter Γ for the same light frequency of 1.55 eV as used in Ref. [26]. For small values of Γ between 25–50 meV the predicted magnitude of the photocurrent lies

in the vicinity of 50 A/m, which is roughly one order of magnitude larger than the magnitude of photocurrents emerging in the magnetic Rashba model with the Rashba strength of 100 meV and similar parameters of the pulse and degree of disorder, as predicted in Ref. [26]. This highlights FGT as a source of strong intrinsic photocurrents which originate in the symmetry properties of this material, and which will emerge in addition to interfacial currents when deposited on a substrate.

The magnitude of the photocurrents rapidly decreases as the amount of disorder increases in the system, and the signal decreases 10-fold by going to the values of Γ of about 300 meV, with J_y changing sign at the disorder strength of about 150 meV. Generally, the overall functional dependence of the photocurrents on lifetime currently presents a subject of debates, as the nonlinear nature of the effect makes it extremely difficult to disentangle various physically distinct disorder-driven contributions to the photocurrents such as, e.g., shift, Berry curvature dipole, jerk, injection, and ballistic currents [36–44]. According to our calculations, which do not assume any approximations on the nature of photoinduced electronic processes, in a large range of Γ beyond 300 meV the photocurrents in FGT exhibit a clear $1/\Gamma$ behavior (see inset of Fig. 2). On the other hand, the behavior found for smaller disorder with respect to Γ appears to be very nonlinear with higher-order contributions clearly at play. Additionally, for polarized along x light, from our calculations we identify J_x and J_y currents as even and odd in Γ, respectively.

In order to examine whether the magnitude of the photocurrents can be controlled by the frequency of the light, we compute relevant components of the conductivity tensor as given by Eq. (3), presenting the results in Fig. 3(a). The calculated signal exhibits a very strong variation with frequency, although the qualitative behavior of the two components is similar. The observed strong variation can be attributed to the complex orbital composition of the electronic structure of FGT. In particular, pronounced variations just below the frequency of 1 and 2 eV can be attributed to the transitions between the groups of bands just above and below the Fermi energy at the K point, and the groups positioned at approximately -1 eV and $+0.5$ eV at the Γ point, which also mediate the behavior of the magneto-optical conductivity of FGT [12,13]. Concerning the overall magnitude of the computed signal, reaching as much as 200 μA/V^2 for frequencies below 1 eV, it is comparable to previously reported results in van der Waals monolayers such as nonmagnetic GeS and WS$_2$ [38,45] and more recently in 2D magnets like CrI$_3$ [46].

The signatures of the orbital structure of FGT can be also clearly seen in the dependence of the photocurrents on band filling, shown in Fig. 3(b). For both components of the currents, the suppression of the signal can be clearly visible for a position of the Fermi energy at about -0.5 and -1.5 eV, which corresponds to the suppression of corresponding transitions, discussed above, as the states become unpopulated with decreasing band filling. Notably, in contrast to J_y, at an energy of ≈ -1.5 eV the sign of J_x changes, which should result in a drastic change in the direction of the in-plane photocurrent. In Fig. 3(c) we plot the band-filling dependence of Q_{zx} and Q_{zy} components of the photocurrents of spin. The predicted magnitude of the spin currents which can be generated by light
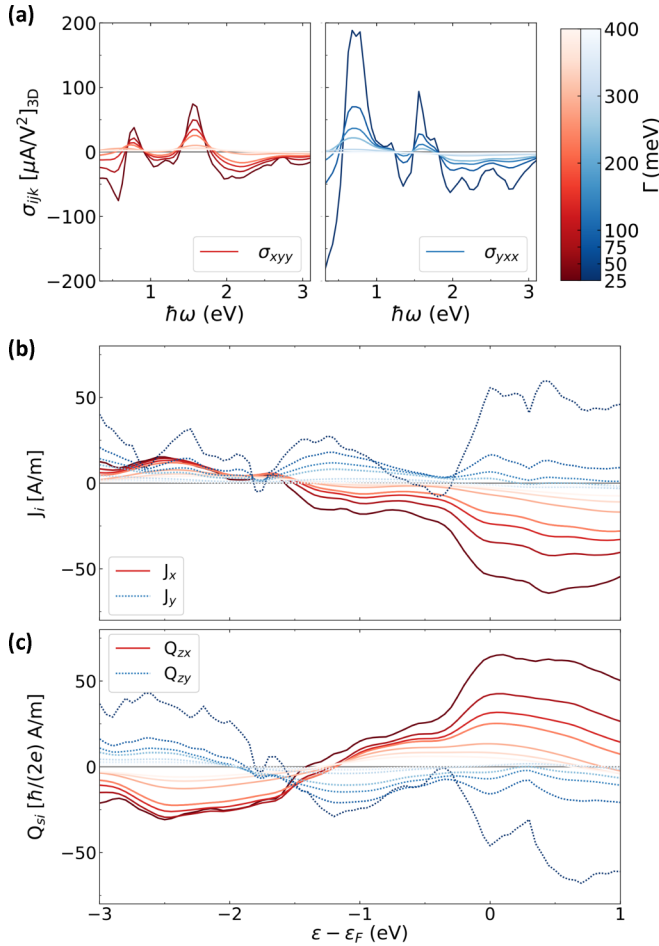
FIG. 3. Spectral properties of the photocurrents. (a) Frequency dependence of the conductivity tensor components σ_{xyy} and σ_{yxx} evaluated for the true position of the Fermi energy in FGT layer for different values of the broadening. (b) Dependence of the photocurrents J_x and J_y on the position of the Fermi level and disorder strength (fading color of the lines). (c) Same as in (a) for spin photocurrents Q_{xz} and Q_{zy}. In (b) and (c) the light pulse of frequency $\hbar\omega = 1.55$ eV and intensity of 10 GW/cm² polarized along the x axis was used. In all plots, Γ is indicated with the color scale.

in FGT is sizable, which marks FGT as one of the promising materials for spin photogalvanic applications.

Interestingly, in a wide energy window just below the true E_F the qualitative behavior of the spin currents is very similar to that of charge currents in terms of the evolution of the magnitude with band filling and dependence on disorder strength. However, one difference is that while Q_{zx} changes sign around -1.5 eV in correlation with J_x, the sign change occurs also for Q_{zy} but not for J_y. This stands in sharp contrast to a simple picture of a spin current being proportional to the spin polarization of the participating states along z, scaled by the corresponding component of the charge photocurrent: indeed, since just below the energy of -1.5 eV the spin polarization of Fe states changes sign, this consideration explains the change in sign of Q_{zx}, however, it fails to mimic the change of sign in Q_{zy}.

To understand this behavior better, we plot the reciprocal space distribution of charge and spin currents at the true
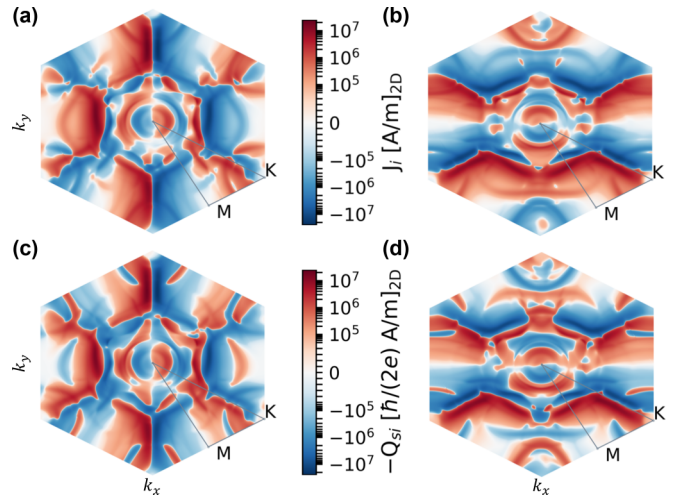

FIG. 4. Reciprocal-space distribution of photocurrents. Distribution of the J_x (a) and J_y (b) charge, and $-Q_{zx}$ (c) and $-Q_{zy}$ (d) spin photocurrents in the Brillouin zone of single-layer FGT computed for the true position of the Fermi energy. The light pulse of frequency $\hbar\omega = 1.55$ eV and intensity of 10 GW/cm² polarized along the x axis was used in combination with disorder strength Γ of 25 meV.

Fermi energy in Fig. 4. While from these plots it is clear that an overall correlation between two types of currents is present, large parts of the Brillouin zone where charge and spin currents have a reversed sign correlation, are also visible, as can be most prominently seen for y components of the currents around the corners of the Brillouin zone. With decreasing band filling the contribution of the corresponding parts becomes promoted, which can explain the change of the sign of Q_{zy} with respect to J_y. Such nontrivial correlation between the magnitude and direction of charge and spin currents can be used to engineer a desired charge and spin transport setup by band filling. We also observe that the decay of the spin photocurrents with disorder strength can depend strongly on the band filling: e.g., while both components of the spin currents decay rapidly with Γ around the true Fermi energy, the Q_{zx} component displays a stronger disorder robustness in the energy region between -3 and -2 eV. This indicates that the direction of spin photocurrents in FGT can be tuned not only by band filling but also by the degree of disorder.

To summarize, in this work we used an *ab initio* implementation of Keldysh formalism for second-order response to address the properties of charge and spin photocurrents in a single-layer Fe₃GeTe₂. Our predictions concerning the symmetry of the currents are in full agreement with direct first-principles calculations, which predict the magnitude of the photocurrents emerging in FGT to be comparable to those of a magnetic Rashba model with strong spin-orbit interaction. The predicted nontrivial response of the currents to such effects as disorder strength, band filling, and frequency marks FGT as a promising platform for crafting the desired properties of the photocurrents, which might prove to be important for future optospintronics applications of 2D magnets.

[1] B. Huang, G. Clark, E. Navarro-Moratalla, D. R. Klein, R. Cheng, K. L. Seyler, D. Zhong, E. Schmidgall, M. A. McGuire, D. H. Cobden, W. Yao, D. Xiao, P. Jarillo-Herrero, and X. Xu, Nature (London) **546**, 270 (2017).

[2] C. Gong and X. Zhang, Science **363**, eaav4450 (2019).

[3] C. Gong, L. Li, Z. Li, H. Ji, A. Stern, Y. Xia, T. Cao, W. Bao, C. Wang, Y. Wang, Z. Q. Qiu, R. J. Cava, S. G. Louie, J. Xia, and X. Zhang, Nature (London) **546**, 265 (2017).

[4] M. Gibertini, M. Koperski, A. F. Morpurgo, and K. S. Novoselov, Nat. Nanotechnol. **14**, 408 (2019).

[5] V. Y. Verchenko, A. A. Tsirlin, A. V. Sobolev, I. A. Presniakov, and A. V. Shevelkov, Inorg. Chem. **54**, 8598 (2015).

[6] B. Ding, Z. Li, G. Xu, H. Li, Z. Hou, E. Liu, X. Xi, F. Xu, Y. Yao, and W. Wang, Nano Lett. **20**, 868 (2020).

[7] Y. Wu, S. Zhang, J. Zhang, W. Wang, Y. L. Zhu, J. Hu, G. Yin, K. Wong, C. Fang, C. Wan, X. Han, Q. Shao, T. Taniguchi, K. Watanabe, J. Zang, Z. Mao, X. Zhang, and K. L. Wang, Nat. Commun. **11**, 3860 (2020).

[8] T.-E. Park, L. Peng, J. Liang, A. Hallal, F. S. Yasin, X. Zhang, K. M. Song, S. J. Kim, K. Kim, M. Weigand, G. Schütz, S. Finizio, J. Raabe, K. Garcia, J. Xia, Y. Zhou, M. Ezawa, X. Liu, J. Chang, H. C. Koo *et al.*, Phys. Rev. B **103**, 104410 (2021).

[9] M. Alghamdi, M. Lohmann, J. Li, P. R. Jothi, Q. Shao, M. Aldosary, T. Su, B. P. T. Fokwa, and J. Shi, Nano Lett. **19**, 4400 (2019).

[10] O. Johansen, V. Risinggård, A. Sudbø, J. Linder, and A. Brataas, Phys. Rev. Lett. **122**, 217203 (2019).

[11] F. Martin, K. Lee, M. Schmitt, A. Liedtke, A. Shahee, H. T. Simensen, T. Scholz, T. G. Saunderson, D. Go, M. Gradhand, Y. Mokrousov, T. Denneulin, A. Kovács, B. Lotsch, A. Brataas, and M. Kläui, Strong bulk spin-orbit torques quantified in the van der Waals ferromagnet Fe_3GeTe_2, arXiv:2107.09420.

[12] X. Yang, X. Zhou, W. Feng, and Y. Yao, Phys. Rev. B **104**, 104427 (2021).

[13] M.-C. Jiang and G.-Y. Guo, Large magneto-optical effect and magnetic anisotropy energy in two-dimensional ferromagnetic metal Fe_3GeTe_2, arXiv:2012.04285.

[14] T. Kampfrath, M. Battiato, P. Maldonado, G. Eilers, J. Nötzold, S. Mährlein, V. Zbarsky, F. Freimuth, Y. Mokrousov, S. Blügel, M. Wolf, I. Radu, P. M. Oppeneer, and M. Münzenberg, Nat. Nanotechnol. **8**, 256 (2013).

[15] S. S. Dhillon, M. S. Vitiello, E. H. Linfield, A. G. Davies, M. C. Hoffmann, J. Booske, C. Paoloni, M. Gensch, P. Weightman, G. P. Williams, E. Castro-Camus, D. R. S. Cumming, F. Simoens, I. Escorcia-Carranza, J. Grant, S. Lucyszyn, M. Kuwata-Gonokami, K. Konishi, M. Koch, C. A. Schmuttenmaer *et al.*, J. Phys. D: Appl. Phys. **50**, 043001 (2017).

[16] M. S. Vitiello, J. Phys.: Mater. **3**, 014008 (2019).

[17] E. T. Papaioannou and R. Beigang, Nanophotonics **10**, 1243 (2021).

[18] M. A. Wahada, E. Sasioglu, W. Hoppe, X. Zhou, H. Deniz, R. Rouzegar, T. Kampfrath, I. Mertig, S. S. P. Parkin, and G. Woltersdorf, Atomic scale control of spin current transmission at interfaces, arXiv:2108.01770.

[19] K. S. Burch, D. Mandrus, and J.-G. Park, Nature (London) **563**, 47 (2018).

[20] T. J. Huisman, R. V. Mikhaylovskiy, J. D. Costa, F. Freimuth, E. Paz, J. Ventura, P. P. Freitas, S. Blügel, Y. Mokrousov, T. Rasing, and A. V. Kimel, Nat. Nanotechnol. **11**, 455 (2016).

[21] J. E. Sipe and A. I. Shkrebtii, Phys. Rev. B **61**, 5337 (2000).

[22] X. Mu, Y. Pan, and J. Zhou, npj Comput. Mater. **7**, 61 (2021).

[23] E. Y. Sherman, A. Najmaie, and J. E. Sipe, Appl. Phys. Lett. **86**, 122103 (2005).

[24] J. Yin and H. Peng, Nat. Nanotechnol. **14**, 105 (2019).

[25] C. Tyznik, J. Lee, J. Sorli, X. Liu, E. K. Holland, C. S. Day, J. E. Anthony, Y.-L. Loo, Z. V. Vardeny, and O. D. Jurchescu, ACS Appl. Mater. Interfaces **13**, 10231 (2021).

[26] F. Freimuth, S. Blügel, and Y. Mokrousov, arXiv:1710.10480 [cond-mat.mes-hall] (2017); Phys. Rev. B **103**, 075428 (2021).

[27] H. Xu, H. Wang, J. Zhou, and J. Li, Nat. Commun. **12**, 4330 (2021).

[28] R.-C. Xiao, D.-F. Shao, Y.-H. Li, and H. Jiang, npj Quantum Mater. **6**, 35 (2021).

[29] M. Berdakin, E. Rodriguez-Mena, and L. Foa Torres, Nano Lett. **21**, 3177.

[30] F. Freimuth, S. Blügel, and Y. Mokrousov, Phys. Rev. B **94**, 144432 (2016).

[31] G. Pizzi, V. Vitale, R. Arita, S. Blügel, F. Freimuth, G. Géranton, M. Gibertini, D. Gresch, C. Johnson, T. Koretsune, J. Ibañez-Azpiroz, H. Lee, J.-M. Lihm, D. Marchand, A. Marrazzo, Y. Mokrousov, J. I. Mustafa, Y. Nohara, Y. Nomura, L. Paulatto *et al.*, J. Phys.: Condens. Matter **32**, 165902 (2020).

[32] F. Freimuth, Y. Mokrousov, D. Wortmann, S. Heinze, and S. Blügel, Phys. Rev. B **78**, 035120 (2008).

[33] X. Wang, J. R. Yates, I. Souza, and D. Vanderbilt, Phys. Rev. B **74**, 195118 (2006).

[34] www.flapw.de.

[35] J. P. Perdew, K. Burke, and M. Ernzerhof, Phys. Rev. Lett. **77**, 3865 (1996).

[36] W. Kraut and R. von Baltz, Phys. Rev. B **19**, 1548 (1979).

[37] V. I. Belinicher and B. I. Sturman, Usp. Fiz. Nauk **130**, 415 (1980) [Sov. Phys.–Usp. **23**, 199 (1980)].

[38] J. Ibañez-Azpiroz, S. S. Tsirkin, and I. Souza, Phys. Rev. B **97**, 245143 (2018).

[39] O. Matsyshyn and I. Sodemann, Phys. Rev. Lett. **123**, 246602 (2019).

[40] T. Morimoto and N. Nagaosa, Sci. Adv. **2**, (2016).

[41] J. Ahn, G.-Y. Guo, and N. Nagaosa, Phys. Rev. X **10**, 041041 (2020).

[42] J. Ahn, G.-Y. Guo, N. Nagaosa, and A. Vishwanath, Riemannian geometry of resonant optical responses, arXiv:2103.01241.

[43] R. Asgari and D. Culcer, Unidirectional valley-contrasting photo-current in the non-linear optical response of transition metal dichalcogenide monolayers, arXiv:2108.10438.

[44] B. I. Sturman, Phys. Usp. **63**, 407 (2020).

[45] C. Wang, X. Liu, L. Kang, B.-L. Gu, Y. Xu, and W. Duan, Phys. Rev. B **96**, 115147 (2017).

[46] Y. Zhang, T. Holder, H. Ishizuka, F. de Juan, N. Nagaosa, C. Felser, and B. Yan, Nat. Commun. **10**, 3783 (2019).